Multiple Aggregation Pathways in Human γS-Crystallin and Its Aggregation-Prone G18V Variant

Kyle W. Roskamp,[1] David M. Montelongo,[1] Chelsea D. Anorma,[1] Diana N. Bandak,[2] Janine A. Chua,[1] Kurtis T. Malecha,[1] and Rachel W. Martin[1,2]

[1]Department of Chemistry, University of California, Irvine, Irvine, California, United States
[2]Department of Molecular Biology and Biochemistry, University of California, Irvine, Irvine, California, United States

Correspondence: Rachel W. Martin, Department of Chemistry, 4136 Natural Sciences 1, University of California, Irvine, Irvine, CA 92697-2025, USA;
rwmartin@uci.edu.

KWR and DMM contributed equally to the work presented here and should therefore be regarded as equivalent authors.

Submitted: August 26, 2016
Accepted: March 17, 2017

Citation: Roskamp KW, Montelongo DM, Anorma CD, et al. Multiple aggregation pathways in human γS-crystallin and its aggregation-prone G18V variant. *Invest Ophthalmol Vis Sci*. 2017;58:2397–2405. DOI: 10.1167/iovs.16-20621

Purpose. Cataract results from the formation of light-scattering precipitates due to point mutations or accumulated damage in the structural crystallins of the eye lens. Although excised cataracts are predominantly amorphous, in vitro studies show that crystallins are capable of adopting a variety of morphologies depending on the preparation method. Here we characterize thermal, pH-dependent, and UV-irradiated aggregates from wild-type human γS-crystallin (γS-WT) and its aggregation-prone variant, γS-G18V.

Methods. Aggregates of γS-WT and γS-G18V were prepared under acidic, neutral, and basic pH conditions and held at 25°C or 37°C for 48 hours. UV-induced aggregates were produced by irradiation with a 355-nm laser. Aggregation and fibril formation were monitored via turbidity and thioflavin T (ThT) assays. Aggregates were characterized using intrinsic aromatic fluorescence, powder x-ray diffraction, and mass spectrometry.

Results. γS-crystallin aggregates displayed different characteristics depending on the preparation method. γS-G18V produced a larger amount of detectable aggregates than did γS-WT and at less-extreme conditions. Aggregates formed under basic and acidic conditions yielded elevated ThT fluorescence; however, aggregates formed at low pH did not produce strongly turbid solutions. UV-induced aggregates produced highly turbid solutions but displayed only moderate ThT fluorescence. X-ray diffraction confirms amyloid character in low-pH samples and UV-irradiated samples, although the relative amounts vary.

Conclusions. γS-G18V demonstrates increased aggregation propensity compared to γS-WT when treated with heat, acid, or UV light. The resulting aggregates differ in their ThT fluorescence and turbidity, suggesting that at least two different aggregation pathways are accessible to both proteins under the conditions tested.

Keywords: crystallins, amyloid fibrils, protein aggregation

Cataract results from aggregation of the structural crystallin proteins of the eye lens. Several aggregation states have been observed in cataract, including fibrils, crystals, and most commonly, amorphous aggregates.[1] In the healthy eye lens, attractive interactions are present among the crystallin proteins, and βγ-crystallins maintain their refractive index gradient through short-range interprotein interactions.[2] Nevertheless, the βγ-crystallins exhibit a very low aggregation propensity, even at the high concentrations present in this specialized tissue.[3] Unmodified wild-type crystallin proteins are extremely stable in the lens environment; however, their solubility is readily compromised by changes in solution conditions, mutations, or posttranslational modifications. Most of the available literature indicates that senile cataract primarily consists of amorphous aggregates[4–8]; however, several studies have shown that crystallins readily fibrillize in vitro under a variety of conditions,[9–15] and amyloid aggregates have been observed in vivo in mouse models of cataract.[16]

In general, protein aggregation has been implicated in numerous diseases as well as in vital cellular processes in organisms ranging from bacteria to humans. Aggregation mechanisms include nonspecific denaturation, native-like assemblies of the monomeric building block, or refolding into an alternate stable state. A wide variety of proteins are known to form amyloid fibrils, in which short β-strands stack upon one another and interact to form a characteristic cross-β structure.[17] This aggregation mechanism has been observed for many proteins, including those that are extremely soluble in their native conformations (e.g., lysozyme),[18,19] leading to the hypothesis that the amyloid fibril state represents a generally stable state that any protein may adopt under appropriate conditions. Fibrillar structures have been observed for bovine α-, β-, and γ-crystallins,[20] as well as γD- and γC-crystallins.[21,22] In γD-crystallin, elevated temperature promotes an increase in fibrillar aggregate formation at acidic pH.[15]

Many protein-deposition diseases are hereditary, with point mutations leading to protein products with reduced solubility. Some sequences are prone to misfolding to form amyloids, as in the case of the mutations causing early-onset Alzheimer's disease.[23] Alternatively, insoluble structures can be assembled from folded monomers having altered intermolecular interactions, as in sickle cell anemia.[24] Point mutations or posttranslational modifications can result in local unfolding, providing hotspots for aggregation despite the retention of all or most native structure.[25–29] At the other extreme, reduced overall stability leads to equilibrium unfolded states that promote

nonspecific denaturation by exposing regions where hydrophobic interactions may occur between monomers, as in familial amyotrophic lateral sclerosis.[30]

To date more than 30 human γ-crystallin mutations have been linked to congenital cataract, including six truncations and two frameshifts (see Vendra et al.).[31,32] Examples for human γD-crystallin include the G61C variant[33] and W42Q variant, which has increased aggregation propensity in the presence of the wild-type protein.[34] In γS-crystallin, the G18V,[35] G57W,[36] and D26G variants are associated with hereditary cataract.[37–39] The focus of the present study is γS-crystallin, the primary protein component in the cortex of the human eye lens and the most conserved of the mammalian crystallins, and its G18V variant. γS-G18V has been shown to be less thermally stable and more aggregation-prone than wild-type. Here we investigate whether the mutation alters the relative populations of different types of aggregates or changes the protein's susceptibility to UV light damage.

Crystallin aggregation can be induced or exacerbated by posttranslational modifications (PTMs) and UV-induced photodamage. UV-induced aggregates are of particular interest because the human eye lens is exposed to incident UV radiation from the sun on a daily basis. Although the cornea absorbs the bulk of the UV radiation reaching the eye, over a lifetime the total UV exposure of the lens is considerable. UV irradiation causes fragmentation and aggregate formation due to cross-linking in bovine β_L-crystallin.[40] This process is inhibited by the chaperone protein α-crystallin in vivo,[41] but as the lens ages, the aggregates accumulate until the chaperone is overwhelmed, resulting in cataract.[42,43] Furthermore, UV-A radiation can cause dimerization and degradation of α-crystallin protein molecules themselves.[44] Many previous studies have focused on UV-B[45] or UV-C[46] irradiation. Here we investigate the effects of UV-A because lens fiber cells are exposed to a large flux of UV-A radiation over time, nearly 100 times greater than UV-B.[47] This potential source of cumulative photodamage is mitigated somewhat by UV-A–filtering metabolites present in the lens; however, wavelengths between 350 and 375 nm are nonetheless also absorbed by γ-crystallins.[48] Direct UV damage of crystallin proteins is implicated in cortical cataract, while the breakdown products of the small-molecule UV filters themselves play a more important role in age-related nuclear cataract.[49] Characterization of the aggregates formed via all of these mechanisms is necessary in order to understand the interaction between protein mutations and environmental effects and to identify appropriate model systems for studying these processes in the laboratory.

Methods

Protein Expression and Purification

Expression and purification of wild-type human γS-crystallin (γS-WT) and γS-G18V was performed as described in Brubaker et al.[37] Briefly, pET28a(+) vectors (Novagen, Darmstadt, Germany) containing γS-WT and γS-G18V cDNA with an N-terminal 6x-His tag and a tobacco etch virus (TEV) protease cleavage sequence were transformed into Rosetta (DE3) *Escherichia coli*. Proteins were then overexpressed using standard isopropyl β-D-1-thiogalactopyranoside induction and lysed via sonication. Cell lysate was loaded on to a Ni-NTA column (Applied Biosystems, Foster City, CA, USA) and eluted using imidazole. His-tags were cleaved by TEV protease (produced in-house) and separated by reapplication to the Ni-NTA column. Finally, proteins were run over a HiLoad 16/600 Superdex 75 pg column (GE Healthcare Life Sciences, Piscataway, NJ, USA) and dialyzed into phosphate buffer (10 mM sodium phosphate, 150 mM NaCl, pH 6.9) prior to use.

Thermal and pH Aggregate Preparation

Purified γS-WT and γS-G18V were prepared at eight pH conditions using carbonate (pH 9), phosphate (pH 2, 3, 6, 7, 8), and acetate (pH 4, 5) buffers at 0.01 M with 150 mM NaCl. Samples were dialyzed by single pH increments over 12-hour periods to their final pH. Next, aliquots of both proteins at 1 mg/mL were prepared and incubated at 25°C or 37°C in a water bath for 48 hours.

UV-A–Induced Aggregation

Both proteins were concentrated to 6 mg/mL in phosphate buffer and filtered with a 0.22-μm filter. Samples were held in a 1-cm pathlength quartz cuvette (Starna Cells, Atascadero, CA, USA) and maintained between 22°C and 24°C using a temperature controller (Quantum Northwest Luma 40/Eclipse with Peletier element and recirculator; Quantum Northwest Inc., Liberty Lake, WA, USA). Continuous stirring was maintained throughout the experiment, with 100-μL aliquots taken every 10 minutes for 90 minutes. UV-A irradiation was produced using a 20 Hz Nd:YAG laser (Continuum Surelite II; Surelite, San Jose, CA, USA) coupled to a Surelite Separation Package (SSP) 2A (Surelite) to change the pump laser wavelength (1064 nm) to 355 nm via third harmonic generation. The laser flux was 89 mJ/cm^2 at 10 Hz.

Turbidity Measurements

UV-irradiated samples were diluted with phosphate buffer to a concentration of 1 mg/mL. Samples were resuspended immediately prior to measurement in which 400-μL aliquots were loaded into a 1-cm pathlength quartz cuvette and measured using a spectrophotometer (JASCO V-730 UV-Vis; Jasco Analytical Instruments, Easton, MD, USA). The measured absorbance at 600 nm was used as the turbidity value.

Thioflavin T and Aromatic Fluorescence

To investigate amyloid fibril character, thioflavin T (ThT) assays were conducted as described by Nilsson et al.[50] A ThT working solution (25 μM ThT, 10 mM phosphate, 150 mM NaCl, pH 7) was prepared the day of analysis and used as a reference blank for all measurements. Aliquots (50 uL) of thermal or UV-treated protein were mixed with the ThT working solution to prepare 0.05 mg/mL samples for analysis. Fluorescence was recorded using a Gemini EM Microplate Reader (Molecular Devices, Sunnyvale, CA, USA) with 440 nm excitation and 482 nm emission. Measurements were performed in triplicate.

Intrinsic γS-crystallin tryptophan (Trp) fluorescence was measured using an excitation wavelength of 280 nm and emission range from 310 to 400 nm, in the instrument described above.

X-ray Diffraction

Aggregates were prepared for diffraction experiments by adding glycerol to the protein samples to a final concentration of 50% by volume. Each sample was mounted on a loop and frozen using a cryogenic nitrogen gas stream. X-ray diffraction data were collected using an in-house Rigaku MicroMax 007 rotating anode for x-ray generation and detected with a Saturn 944 detector (Crystal Logic, Los Angeles, CA, USA). Samples exhibiting diffraction bands corresponding to approximately 4.7 and 10 Å in real space contain amyloid fibrils. Lysozyme

Investigative Ophthalmology & Visual Science

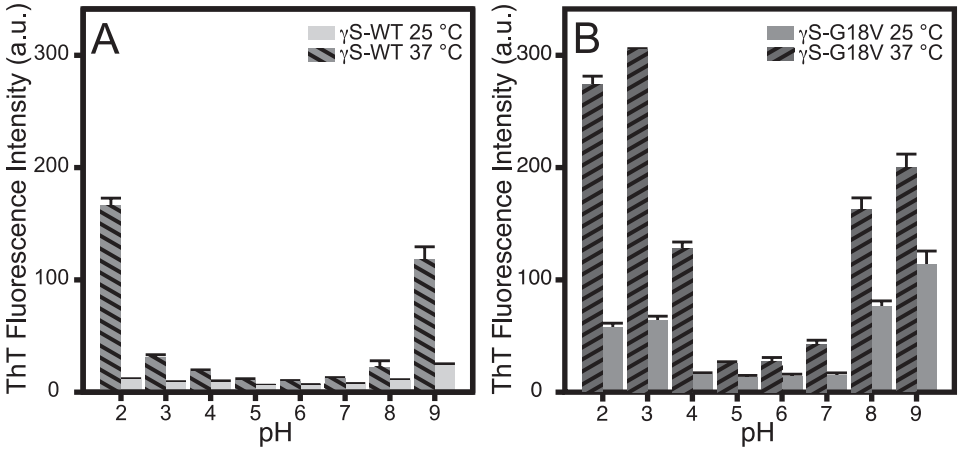

Figure 1. ThT fluorescence of γS-WT and γS-G18V prepared at variable pH and two temperatures. (**A**) For γS-WT at 25°C, only background fluorescence is observed. For γS-G18V, elevated ThT fluorescence is observed at both low (2–3) and high (8–9) pH. Only heated samples (37°C) at pH 2 and 9 exhibit elevated fluorescence. (**B**) At physiological temperature (37°C), elevated ThT fluorescence is seen in γS-WT at pH 2 and 9, while γS-G18V displays significant increases in signal at pH 2, 3, 8, and 9.

amyloid fibril samples prepared according to Xu et al. were used as a positive control.[51]

Matrix Assisted Laser Desorption Ionization-Time of Flight (MALDI-TOF) Mass Spectrometry

UV-irradiated and unexposed proteins were digested using MS Grade Pierce Trypsin Protease (ThermoFischer Scientific, Rockford, IL, USA) at 37°C. The digest was mixed with saturated solution of α-cyano-4-hydrocinnamic acid in 50% acetonitrile and 1% trifluoroacetic acid and spotted onto a dry plate. MALDI-TOF analysis was performed using an AB SCIEX TOF/TOF 5800 System (SCIEX, Foster City, CA, USA and the resulting masses were referenced against the fragments predicted by Protein Prospector MS-Digest[52] (http://prospector.ucsf.edu, in the public domain).

Results

In order to measure the effects of pH on aggregate formation, the pH of γS-WT and γS-G18V solutions was varied over the range 2 through 9 while incubating the samples at room temperature (25°C) and physiological temperature (37°C). The ThT fluorescence of γS-WT and γS-G18V under all pH and both temperature conditions is summarized in Figure 1. Trace ThT fluorescence is observed for γS-WT held at 25°C under all conditions examined, while for γS-G18V, elevated ThT fluorescence is observed at both low (2–3) and high (8–9) pH values (Fig. 1A). At 37°C, samples of γS-WT incubated at pH 2 and 9 exhibit dramatic increases in fluorescence, while only minimal increases are observed at all remaining pH conditions. In contrast, γS-G18V exhibits elevated fluorescence over a larger pH range (pH 2–4 and 8–9). Roughly a 5-fold increase in ThT fluorescence is observed under acidic conditions (pH 2, 3, 4), while the signals observed from samples heated under basic conditions double in intensity. At 37°C, γS-WT likewise displays a greater increase in ThT fluorescence at pH 2 than at pH 9.

In order to determine whether other aggregates were present that did not produce the elevated ThT fluorescence consistent with amyloid fibril formation, the solution turbidity was measured as the optical density at 600 nm (Fig. 2). For γS-WT, increased turbidity was observed only at pH 9, despite increased ThT fluorescence at pH 2 and 9. The turbidity of γS-WT at pH 9 was roughly half that observed for γS-G18V under

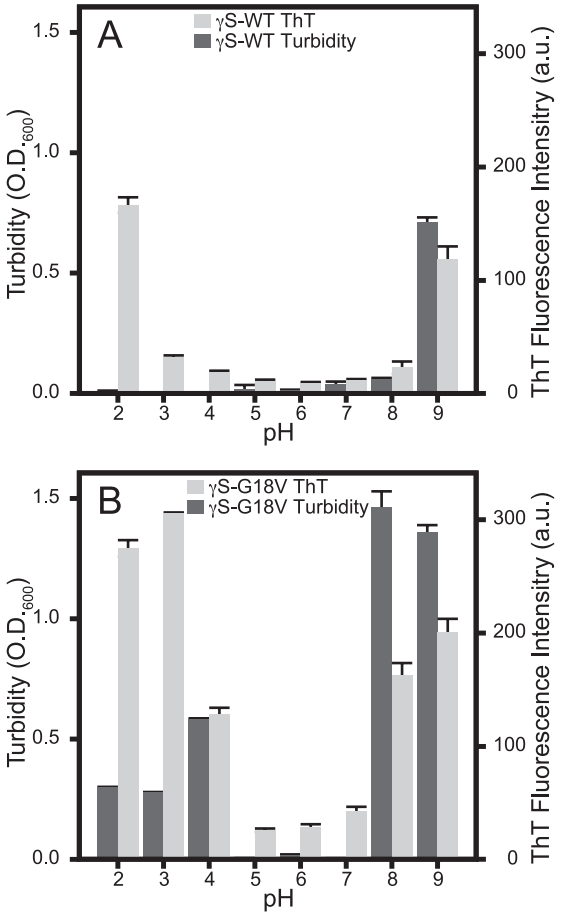

Figure 2. The ThT fluorescence and turbidity of γS-WT (**A**) and γS-G18V (**B**) from samples incubated at 37°C plotted by pH. (**A**) Minimal γS-WT ThT fluorescence (*light gray*) and turbidity (*dark gray*) are observed over the pH range of 3 through 8. At pH 2, only ThT fluorescence increases, while both turbidity and ThT fluorescence increase at pH 9. (**B**) In γS-G18V, ThT fluorescence (*light gray*) and turbidity (*dark gray*) are elevated at basic and acidic conditions (pH 2, 3, 4, 8, 9). Acidic conditions result in the greatest γS-G18V ThT fluorescence levels, while basic conditions result in the greatest turbidity for γS-G18V. In both assays, only minimal changes are observed under neutral to weakly acidic conditions (pH 5, 6, 7).

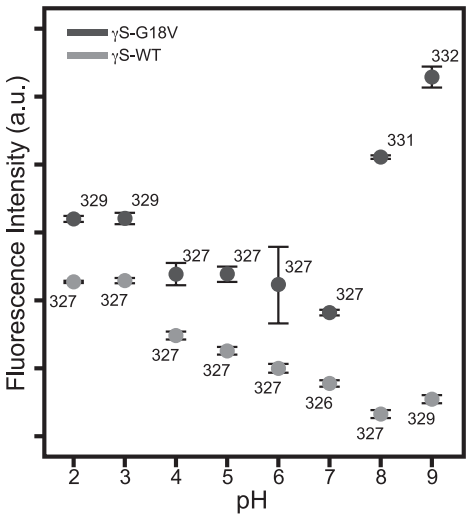

Figure 3. The intrinsic Trp fluorescence intensity for γS-WT (*light gray*) and γS-G18V (*dark gray*) at different pH values. The wavelength of the emission maximum is labeled next to each data point. Greater fluorescence for both proteins occurs under acidic conditions, with slight redshifting of the emission maxima for γS-G18V at pH 2 and 3. Under basic conditions, γS-G18V produces the greatest fluorescence intensity and maximum redshift, whereas the fluorescence intensity of γS-WT changes minimally and redshifts only slightly at pH 9.

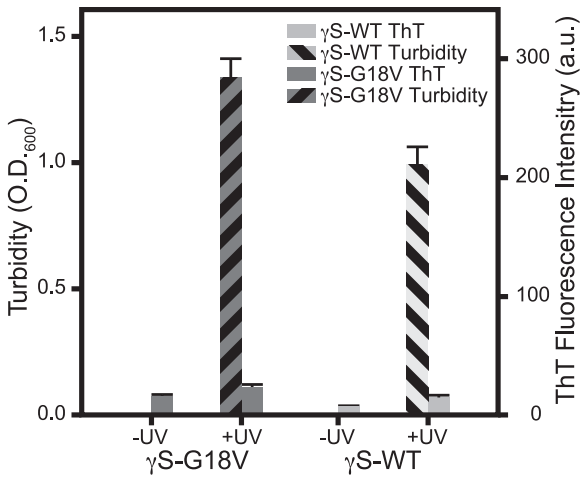

Figure 4. ThT fluorescence and turbidity measurements of γS-WT and γS-G18V at pH 7, before (–UV) and after (+UV) exposure to UV-A irradiation for 90 minutes. In both proteins, untreated samples display negligible ThT fluorescence and turbidity. UV-A irradiation produces significantly elevated turbidity, but only minimal increases in ThT fluorescence.

the same conditions. Increased turbidity for γS-G18V was greatest at pH 8 and 9, but also was elevated compared to neutral conditions at pH 2, 3, and 4.

The intrinsic Trp fluorescence of γS-WT and γS-G18V was measured in order to assess the degree of structural disruption to the crystallin fold upon changing the pH. Partial unfolding and changes to the local environment surrounding Trp residues alter the spectrum in both λ_{max} and intensity. In more polar environments, the Trp fluorescence maximum occurs at a longer wavelength; therefore, redshifting of the fluorescence peak indicates changes in conformation consistent with increased solvent exposure of the Trp residues. Trp fluorescence results are summarized in Figure 3, while the full spectra for γS-WT and γS-G18V from pH 2 to 9 are shown in Supplementary Figure S1. The total Trp fluorescence signal decreases from pH 2 to 7 for both proteins, with only a slight redshift occurring for the fluorescence maxima at pH 2 and 3 in γS-G18V. Increased quenching is observed at pH 8 for γS-WT, and at pH 9 slight redshifting is also observed. The γS-G18V fluorescence signals at pH 8 and 9 are the most intense and redshifted observed for either protein, indicating that G18V is vulnerable to structural disruption at high pH, while γS-WT maintains the integrity of its fold over a wide range of solution conditions.

Aggregation of both γS-WT and γS-G18V was induced via UV-A irradiation at neutral pH and monitored using turbidity and ThT fluorescence. Samples of both proteins were irradiated for 90 minutes, at which point increases in solution turbidity leveled off (Supplementary Fig. S2). Both proteins exhibit large increases in turbidity following UV-A exposure. As for the samples incubated at physiological temperature, more aggregation is observed for γS-G18V than for γS-WT (Fig. 4). In the case of both proteins, the UV-exposed samples exhibit only small increases in ThT fluorescence, suggesting that amyloid fibrils are not the primary aggregation product produced under UV-A irradiation.

X-ray diffraction experiments were performed on low-pH and UV-treated γS-WT and γS-G18V in order to characterize the nature of the aggregates. Representative diffraction patterns are shown in Figure 5. Image analysis was conducted on a horizontal slice of the image, and all relevant peaks in the image intensity profile were labeled with their corresponding real-space resolution measurement, in angstrom units. The principal signals observed were sharp rings at 4.7 Å and broader rings at 10–11 Å.

PTMs from UV-A photodamage were identified using MALDI-TOF mass spectrometry of trypsin-digested samples after 90 minutes of irradiation. Modifications were considered to be caused by UV-A irradiation if both the modified and unmodified fragments were observed and the peak corresponding to the modified fragment was uniquely observed in the UV-irradiated sample. Mass differences corresponding to deamidation (m + 1), oxidation (m + 16, m + 32), and Trp modifications such as kynurenine (m + 4) were observed in both proteins (Fig. 6).

Discussion

Several pathways have been proposed to explain the mechanism of γ-crystallin aggregation.[53–57] Photochemical damage has been shown to cause intermolecular cross-linking, which may increase noncovalent aggregation due to redistributed charge altering the proteins' isoelectric points.[53] UV exposure may also produce reactive oxygen species via Fenton chemistry, resulting in nonspecific oxidation and cross-linking.[58] Other nonspecific PTMs such as glycation,[59] acetylation,[60] and deamidation[61] may destabilize the protein structure, similar to the effects of point mutations.[32,62–65] Unfolding within either domain or at the domain interface may lead to different domain-swapped aggregation pathways,[34] precede amyloid fibril formation,[10] or result in nonspecific aggregation.[66–68] Furthermore, two or more of these pathways may be in competition under a particular set of conditions, as is observed for both γS-WT and γS-G18V.

From these data, it is clear that low-pH conditions are necessary for γS-WT to form amyloid fibrils at physiological temperature. Under every other condition that was tested, the samples remained translucent with no visible signs of aggregation, and there was little to no increase in ThT fluorescence intensity, indicating the absence of β-amyloid

Investigative Ophthalmology & Visual Science

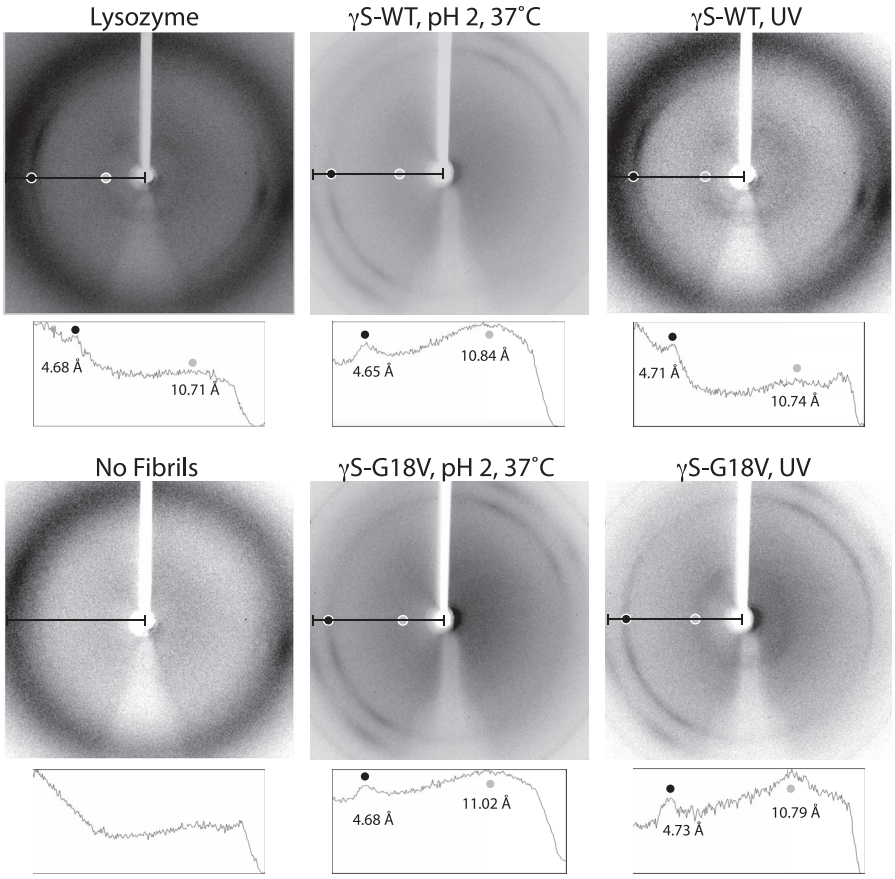

Figure 5. Representative x-ray diffraction patterns for fibrillar aggregates of γS-WT and γS-G18V. Lysozyme fibrils prepared by incubation at 60°C and pH 2 for 2 days prior to the experiment were used as a positive control. Below each image, its corresponding image intensity profile is shown for the area of the image designated with a *black line*. Relevant peaks are labeled with their resolution measurement, in angstrom units, and the location of each peak is correlated to the location on the diffraction pattern with *light gray* or *dark gray dots*.

structure. This result is not surprising given that γS-WT is a highly stable protein that has been selected for a very low propensity to aggregate, even under harsh conditions. By contrast, γS-G18V exhibits large increases in ThT fluorescence intensity under conditions where none was observed for γS-WT. For γS-G18V, increased ThT fluorescence signals were observed in all samples incubated at 37°C, save for the pH 7 sample, and in two of the room-temperature samples as well (pH 2 and pH 9).

Although increased ThT fluorescence intensity was not observed in the γS-G18V pH 4, 25°C sample or the pH 7, 37°C sample, the incubated samples had visibly aggregated at the time of the fluorescence measurement, indicating the formation of nonamyloid aggregates and supporting the hypothesis that more than one aggregation state is available to γS-crystallin. The increase in turbidity seen in these two samples without an accompanying increase in ThT fluorescence indicates that these aggregates are not fibrillar and instead adopt a more disordered aggregation state. Likewise, for γS-WT incubated at pH 2, strong ThT fluorescence but only weak turbidity were observed, consistent with reports for γD-crystallin under similar conditions.[15] Similar changes were observed for γS-G18V at pH 2 and 3. However, correlated increases in ThT fluorescence and turbidity were seen for γS-WT at pH 9 and γS-G18V at pH 4, 8, and 9, indicating that the pH strongly influences the balance of different aggregation states.

Intrinsic Trp fluorescence was used to assess the degree of protein unfolding implicated in these different aggregation pathways. Trp fluorescence is a sensitive probe of native structure in this system because each Greek key domain contains two critical Trp residues in its hydrophobic core. These residues absorb UV-B light and are thought to participate in a proposed fluorescence resonance energy transfer quenching mechanism to dissipate energy that might otherwise damage the lens or retina.[69–71] The intrinsic aromatic Förster of γS-WT and γS-G18V showed similar quenching patterns under acidic (pH 2) to neutral (pH 7) conditions, with a slight redshift in the signal for γS-G18V under acidic conditions. The reduction in fluorescence quenching under acidic conditions may be correlated with changes in the protonation states of carboxyl side chains, which can disrupt hydrogen-bonding interactions and salt bridges. Under mildly basic conditions (pH 8 and 9), γS-G18V exhibits a larger redshift of 4–5 nm, along with significant increases in fluorescence compared to pH 7. For γS-WT, only minor changes are observed, even at pH 9.

In γS-G18V, significant structural changes are apparent from the large redshift at pH 8–9. These may be related to changes in cysteine protonation (pKa ~8) and are consistent with the large structural rearrangement of the area around the cysteine loop of γS-G18V relative to that of γS-WT, as observed in the solution-nuclear magnetic resonance structures (Protein Data Bank ID 2M3U and 2M3T).[65] These data suggest that basic pH conditions favor partial unfolding of γS-G18V, while γS-WT does not appear to experience even partial unfolding under any conditions tested here. The observed redshifts in the Trp fluorescence maxima correlate with the increased optical

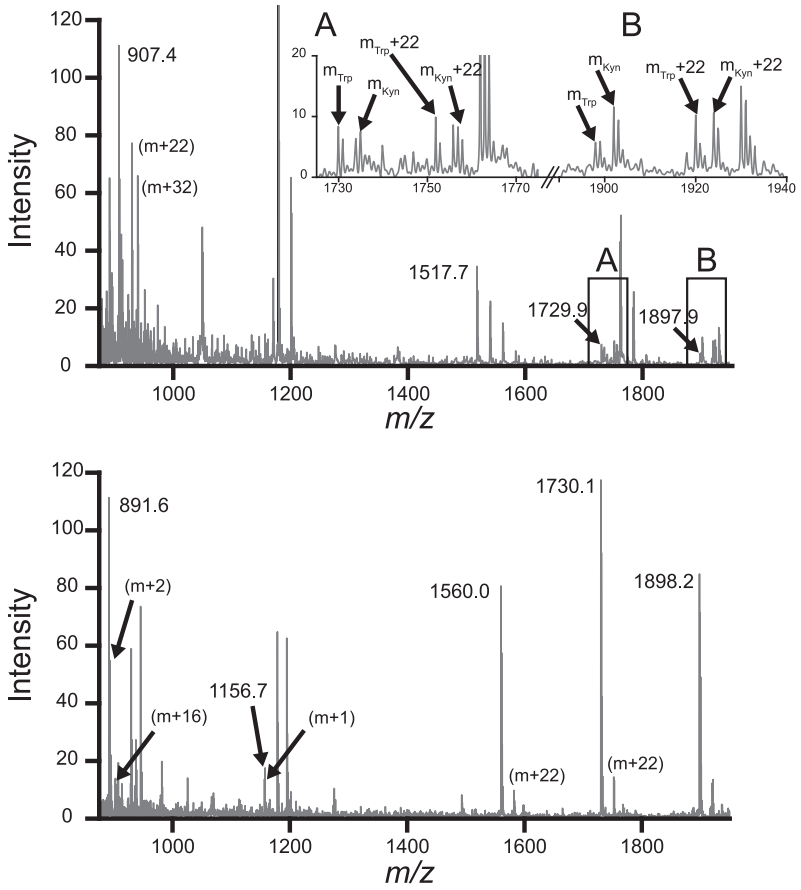

Figure 6. Representative MALDI-TOF spectra of trypsin-digested samples of γS-WT and γS-G18V after UV-A irradiation. Mass fragments were identified by manual comparison of mass-to-charge ratio peaks to the theoretical peaks and isotopic mass distributions from MS-Digest (http://prospector.ucsf.edu, in the public domain). Additional mass fragments corresponding to identifiable molecular weight changes are labeled with the specific mass difference, that is, m + 16. *Top*: The γS-WT spectrum is shown with selected fragments annotated. Insets **A** and **B** display the observed cases of m + 4 peaks in matched fragments containing a Trp residue. An m + 4 mass difference matches a Trp-to-Kyn PTM. The masses for each peak are labeled as m_{Trp} and m_{Kyn}. *Bottom*: The γS-G18V distribution is shown with annotations indicating each of the observed peaks matching an MS-Digest fragment. Kyn, kynurenine.

densities: γS-G18V at pH 8 and 9 are the most turbid and display the greatest redshifts, while γS-WT at pH 9 and γS-G18V at pH 2 and 3 exhibit smaller redshifts and reduced optical density.

UV-A irradiation was also explored as a more biologically relevant mechanism of aggregation initiation. In our experiments, prolonged irradiation resulted in elevated solution turbidity, yet produced weaker ThT fluorescence than samples treated under acidic and basic conditions at physiological temperature. The minimal ThT fluorescence and elevated turbidity of UV-irradiated samples is most comparable to thermally treated γS-WT and γS-G18V under basic conditions. The reduced ThT response following the initial turbidity increases correlated with visible yellowing in irradiated sample precipitates, which were initially white, but progressively darkened with UV exposure.

To identify some of the protein modifications produced via UV-A exposure, endpoint samples were digested using trypsin and analyzed via MALDI-TOF mass spectrometry. The resulting data were compared to theoretical molecular weight values predicted by Protein Prospector MS-Digest with modifications reported from mass spectrometry analysis of cataractous lenses.[72,73] Deamidation and oxidation products were both observed, consistent with literature reports of digested normal and cataract lenses.[60,74] In particular, mass differences of 4 and 20 Da were observed, suggesting the presence of the tryptophan oxidation products kynurenine and *N*-formylkynurenine. This result is consistent with the yellowing of the UV aggregates over time, because kynurenine absorbs blue light, contributing to the color changes ranging from yellowing to browning often seen in aged lenses.[74]

To test for the presence of amyloid fibril character in our different aggregates, x-ray diffraction experiments were conducted. Powder diffraction techniques can be utilized to gain structural information about the degree of local order in solid samples. Diffraction patterns of noncrystalline structures can yield valuable information about the average distances between molecules. Due to the repeating cross-β structure of the fibril, the appearance of characteristic diffraction bands in the reciprocal space diffraction pattern corresponding to 4.7 and 10 Å in real space will be observed in samples containing amyloid fibrils. These distances represent the interstrand distance between β-strands along the fibril axis and the intersheet spacing distance within the fibril, respectively. Powder x-ray diffraction (representative data shown in Fig. 5) indicates that amyloid fibrils were detectable even under conditions that produced only weak ThT fluorescence, in this case UV-irradiated samples at neutral pH.

The results of these experiments support the hypothesis that there are at least two aggregation states available to both

γS-WT and γS-G18V. One of these states is a disordered aggregate with little to no amyloid fibril character, which nonetheless results in the opacification of the sample, as seen through the increase in turbidity without an increase in ThT fluorescence or the amyloid fibril diffraction bands in the x-ray diffraction pattern. The second state has significant amyloid fibril character, as shown in both the increased ThT fluorescence and the appearance of the fibril diffraction bands in the x-ray diffraction experiments. The γS-G18V variant samples formed this second type of aggregate more readily, and under a broader range of conditions than the WT protein. UV-A exposure at neutral pH leads to aggregation as indicated by increased solution turbidity. Although only a weak ThT response is observed in these samples, amyloid fibril character is confirmed via powder x-ray diffraction. Taken together, these data suggest that changing the solution can shift the population of the two aggregation states to favor one or the other, but both forms are detectable under all conditions where aggregation was observed.

The visible coloration of UV samples provides a clue that photodamage may occur during UV-A exposure. MALDI-TOF mass spectrometry of digested samples of UV-A–irradiated γS-WT and γS-G18V confirmed but does not inform us about, the mechanism driving aggregation or differentiate it from similar results produced via other methods; further studies are needed to elucidate the mechanisms underlying these disparate aggregation pathways.

Conclusions

Our results indicate that multiple aggregation pathways are accessible to both wild-type γS-crystallin and its aggregation-prone G18V variant. The method used to initiate aggregation strongly determines the relative populations of the two types of aggregates, although both types are present under the conditions tested. The disease-related variant forms more aggregates than wild-type, and under milder conditions, but it does not apparently favor a particular type of aggregate. Future studies will focus on further characterization of the aggregates induced by UV-A irradiation.

Acknowledgments

The authors thank D. Fishman and F. Grun for excellent management of the UCI Optical Spectroscopy facility and the UCI Mass Spectrometry facility, respectively. The authors also thank S. Nizkorodov and T. Poulos for allowing the use of instrumentation in their labs, and G. Chreifi for his assistance with x-ray diffraction experiments.

Supported by National Institutes of Health Grants 1R01 EY021514 and 1R01 EY025328, and National Science Foundation Grant DMS-1361425.

Disclosure: **K.W. Roskamp**, None; **D.M. Montelongo**, None; **C.D. Anorma**, None; **D.N. Bandak**, None; **J.A. Chua**, None; **K.T. Malecha**, None; **R.W. Martin**, None

References

1. Serebryany E, King JA. The βγ-crystallins: native state stability and pathways to aggregation. *Prog Biophys Mol Biol*. 2014; 115:32–41.
2. Delaye M, Tardieu A. Short-range order of crystallin proteins accounts for eye lens transparency. *Nature*. 1983;302:415–417.
3. Tardieu A, Vérétout F, Krop B, Slingsby C. Protein interactions in the calf eye lens: interactions between beta-crystallins are repulsive whereas in gamma-crystallins they are attractive. *Eur Biophys J*. 1992;21:1–12.
4. Sandilands A, Hutcheson AM, Long HA, et al. Altered aggregation properties of mutant γ-crystallins cause inherited cataract. *EMBO J*. 2002;21:6005–6014.
5. Moncaster JA, Pineda R, Moir RD, et al. Alzheimer's disease amyloid-β links lens and brain pathology in down syndrome. *PLoS One*. 2010;5:e10659.
6. Goldstein LE, Muffat JA, Cherny RA, et al. Cytosolic β-amyloid deposition and supranuclear cataracts in lenses from people with Alzheimer's disease. *Lancet*. 2003;361:1258–1265.
7. Frederikse PH. Amyloid-like protein structure in mammalian ocular lenses. *Curr Eye Res*. 2000;20:462–468.
8. Michael R, Rosandić J, Montenegro GA, et al. Absence of beta-amyloid in cortical cataracts of donors with and without Alzheimer's disease. *Exp Eye Res*. 2013;106:5–13.
9. Wang Y, Petty S, Trojanowski A, et al. Formation of amyloid fibrils in vitro from partially unfolded intermediates of human γC-crystallin. *Invest Ophthalmol Vis Sci*. 2010;51: 672–678.
10. Papanikolopoulou K, Mills-Henry I, Thol SL, et al. Formation of amyloid fibrils in vitro by human gammaD-crystallin and its isolated domains. *Mol Vis*. 2008;14:81–89.
11. Kosinski-Collins MS, King J. In vitro unfolding, refolding, and polymerization of human γD crystallin, a protein involved in cataract formation. *Protein Sci*. 2003;12:480–490.
12. Moran SD, Zhang TO, Decatur SM, Zanni MT. Amyloid fiber formation in human γD-crystallin induced by UV-B photodamage. *Biochemistry*. 2013;52:6169–6181.
13. Moran SD, Zhang TO, Zanni MT. An alternative structural isoform in amyloid-like aggregates formed from thermally denatured human γD-crystallin. *Prot Sci*. 2014;23:321–331.
14. Moran SD, Decatur SM, Zanni MT. Structural and sequence analysis of the human γD-crystallin amyloid fibril core using 2D IR spectroscopy, segmental 13C labeling, and mass spectrometry. *J Am Chem Soc*. 2012;134:18410–18416.
15. Wu JW, Chen M-E, Wen W-S, et al. Comparative analysis of human γD-crystallin aggregation under physiological and low pH conditions. *PLoS One*. 2014;9:e112309.
16. Sandilands A, Hutcheson AM, Long HA, et al. Altered aggregation properties of mutant gamma-crystallins cause inherited cataract. *EMBO J*. 2002;21:6005–6014.
17. Chiti F, Dobson CM. Protein misfolding, functional amyloid, and human disease. *Annu Rev Biochem*. 2006;75:333–366.
18. Booth DR, Sunde M, Bellotti V, et al. Instability, unfolding and aggregation of human lysozyme variants underlying amyloid fibrillogenesis. *Nature*. 1997;385:787–793.
19. Pepys MB, Hawkins PN, Booth DR, et al. Human lysozyme gene mutations cause hereditary systemic amyloidosis. *Nature*. 1993;362:553–557.
20. Meehan S, Berry Y, Luisi B, Dobson CM, Carver JA, MacPhee CE. Amyloid fibril formation by lens crystallin proteins and its implications for cataract formation. *J Biol Chem*. 2004;279: 3413–3419.
21. Papanikolopoulou K, Mills-Henry I, Thol SL, et al. Formation of amyloid fibrils in vitro by human gammaD-crystallin and its isolated domains. *Mol Vis*. 2008;14:81–89.
22. Wang Y, Petty S, Trojanowski A, et al. Formation of amyloid fibrils in vitro from partially unfolded intermediates of human gammaC-crystallin. *Invest Ophthalmol Vis Sci*. 2010;51:672–678.
23. Cacacea R, Sleegersa K, Van Broeckhoven C. Molecular genetics of early-onset Alzheimer's disease revisited. *Alzheimers Dement*. 2016;12:733–748.
24. Pauling L, Itano HA, Singer SJ, Wells IC. Sickle cell anemia, a molecular disease. *Science*. 1949;110:543–548.

25. Chiti F, Dobson CM. Amyloid formation by globular proteins under native conditions. *Nat Chem Biol*. 2009;5:15–22.
26. Eakin CM, Attenello FJ, Morgan CJ, Miranker AD. Oligomeric assembly of native-like precursors precedes amyloid formation by β-2 microglobulin. *Biochemistry*. 2004;43:7808–7815.
27. Sanders A, Craven CJ, Higgins LD, et al. Cystatin forms a tetramer through structural rearrangement of domain-swapped dimers prior to amyloidogenesis. *J Mol Biol*. 2004; 336:165–178.
28. Liu Y, Gotte G, Libonati M, Eisenberg D. A domain-swapped RNase A dimer with implications for amyloid formation. *Nat Struct Mol Biol*. 2001;8:211–214.
29. Sinha N, Tsai C-J, Nussinov R. A proposed structural model for amyloid fibril elongation: domain swapping forms an interdigitating β-structure polymer. *Protein Eng*. 2001;14:93–103.
30. Kerman A, Liu HN, Croul S, et al. Amyotrophic lateral sclerosis is a non-amyloid disease in which extensive misfolding of SOD1 is unique to the familial form. *Acta Neuropathol*. 2010; 119:335–344.
31. Vendra VPR, Khan I, Chandani S, Muniyandi A, Balasubramanian D. Gamma crystallins of the human eye lens. *Biochim Biophys Acta*. 2016;1860:333–343.
32. Vendra VPR, Agarwal G, Chandani S, Talla V, Srinivasan N, Balasubramanian D. Structural integrity of the Greek key motif in βγ-crystallins is vital for central eye lens transparency. *PLoS One*. 2013;8:e70336.
33. Zhang W, Cai H-C, Li F-F, Xi Y-B, Ma X, Yan Y-B. The congenital cataract-linked G61C mutation destabilizes γD-crystallin and promotes non-native aggregation. *PLoS One*. 2011;6:e20564.
34. Serebryany E, King JA. Wild-type human γD-crystallin promotes aggregation of its oxidation-mimicking, misfolding-prone W42Q mutant. *J Biol Chem*. 2015;290:11491–11503.
35. Sun H, Ma Z, Li Y, et al. Gamma-S crystallin gene (CRYGS) mutation causes dominant progressive cortical cataract in humans. *J Med Genet*. 2005;42:706–710.
36. Khan I, Chandani S, Balasubramanian D. Structural study of the G57W mutant of human gamma-S-crystallin, associated with congenital cataract. *Mol Vis*. 2016;22:771–782.
37. Brubaker WD, Freites JA, Golchert KJ, et al. Separating instability from aggregation propensity in γS-crystallin variants. *Biophys J*. 2011;100:498–506.
38. Karri S, Kasetti RB, Vendra VPR, Chandani S, Balasubramanian D. Structural analysis of the mutant protein D26G of human γS-crystallin, associated with Coppock cataract. *Mol Vis*. 2013;19:1231–1237.
39. Ma Z, Piszczek G, Wingfield PT, Sergeev YV, Hejtmancik JF. The G18V CRYGS mutation associated with human cataracts increases gammaS-crystallin sensitivity to thermal and chemical stress. *Biochemistry*. 2009;48:7334–7341.
40. Muranov KO, Maloletkina OI, Poliansky NB, et al. Mechanism of aggregation of UV-irradiated β(L)-crystallin. *Exp Eye Res*. 2011;92:76–86.
41. Borkman RF, Knight G, Obi B. The molecular chaperone alpha-crystallin inhibits UV-induced protein aggregation. *Exp Eye Res*. 1996;62:141–148.
42. Moreau KL, King JA. Protein misfolding and aggregation in cataract disease and prospects for prevention. *Trends Mol Med*. 2012;18:273–282.
43. Michiel M, Duprat E, Skouri-Panet F, et al. Aggregation of deamidated human βB2-crystallin and incomplete rescue by α-crystallin chaperone. *Exp Eye Res*. 2010;90:688–698.
44. Mafia K, Gupta R, Kirk M, Wilson L, Srivastava O, Barnes S. UV-A-induced structural and functional changes in human lens deamidated αB-crystallin. *Mol Vis*. 2008;14:234–248.
45. Moran SD, Zhang TO, Decatur SM, Zanni MT. Amyloid fiber formation in human γD-Crystallin induced by UV-B photodamage. *Biochemistry*. 2013;52:6169–6181.
46. Wang SS-S, Wen W-S. Examining the influence of ultraviolet C irradiation on recombinant human γD-crystallin. *Mol Vis*. 2010;16:2777–2790.
47. Zigman S. Environmental near-UV radiation and cataracts. *Optom Vis Sci*. 1995;72:899–901.
48. Bessems G, Keizer E, Wollensak J, Hoenders H. Non-tryptophan fluorescence of crystallins from normal and cataractous human lenses. *Invest Ophthalmol Vis Sci*. 1987; 28:1157–1163.
49. Truscott RJW. Human cataract: the mechanisms responsible; light and butterfly eyes. *The Int J Biochem Cell Biol*. 2003;35: 1500–1504.
50. Nilsson MR. Techniques to study amyloid fibril formation in vitro. *Methods*. 2004;34:151–160.
51. Xu M, Ermolenkov VV, Uversky VN, Lednev IK. Hen egg white lysozyme fibrillation: a deep-UV resonance Raman spectroscopic study. *J Biophotonics*. 2008;1:215–229.
52. Chalkley RJ, Hansen KC, Baldwin MA. Bioinformatic methods to exploit mass spectrometric data for proteomic applications. *Methods Enzymol*. 2005;402:289–312.
53. Li D-Y, Borkman RF, Wang R-H, Dillon J. Mechanisms of photochemically produced turbidity in lens protein solutions. *Exp Eye Res*. 1990;51:663–669.
54. Flaugh SL, Kosinski-Collins MS, King J. Contributions of hydrophobic domain interface interactions to the folding and stability of human γD-crystallin. *Prot Sci*. 2005;14:569–581.
55. Naeem A, Fazili NA. Defective protein folding and aggregation as the basis of neurodegenerative diseases: the darker aspect of proteins. *Cell Biochem Biophys*. 2011;61:237–250.
56. Serebryany E, King JA. The βγ-crystallins: native state stability and pathways to aggregation. *Prog Biophys Mol Biol*. 2014; 115:32–41.
57. Serebryany E, Takata T, Erickson E, Schafheimer N, Wang Y, King JA. Aggregation of Trp> Glu point mutants of human gamma-D crystallin provides a model for hereditary or UV-induced cataract. *Prot Sci*. 2016;25:1115–1128.
58. Truscott RJ. Age-related nuclear cataract—oxidation is the key. *Exp Eye Res*. 2005;80:709–725.
59. Luthra M, Balasubramanian D. Nonenzymatic glycation alters protein structure and stability. A study of two eye lens crystallins. *J Biol Chem*. 1993;268:18119–18127.
60. Wilmarth P, Tanner S, Dasari S, et al. Age-related changes in human crystallins determined from comparative analysis of post-translational modifications in young and aged lens: does deamidation contribute to crystallin insolubility? *J Proteome Res*. 2006;5:2554–2566.
61. Hanson SR, Smith DL, Smith JB. Deamidation and disulfide bonding in human lens γ-crystallins. *Exp Eye Res*. 1998;67: 301–312.
62. Li XQ, Cai HC, Zhou SY, et al. A novel mutation impairing the tertiary structure and stability of γC-crystallin (CRYGC) leads to cataract formation in humans and zebrafish lens. *Hum Mutat*. 2012;33:391–401.
63. Bharat SV, Shekhtman A, Pande J. The cataract-associated V41M mutant of human γS-crystallin shows specific structural changes that directly enhance local surface hydrophobicity. *Biochem Biophys Res Commun*. 2014;443:110–114.
64. Vendra VPR, Chandani S, Balasubramanian D. The mutation V42M distorts the compact packing of the human gamma-S-crystallin molecule, resulting in congenital cataract. *PLoS One*. 2012;7:e51401.
65. Brubaker WD, Martin RW. 1H, 13C, and 15N assignments of wild-type human γS-crystallin and its cataract-related variant γS-G18V. *Biomol NMR Assign*. 2012;6:63–67.
66. Kim YH, Kapfer DM, Boekhorst J, et al. Deamidation, but not truncation, decreases the urea stability of a lens structural protein, βB1-crystallin. *Biochemistry*. 2002;41:14076–14084.

Investigative Ophthalmology & Visual Science

67. Lampi KJ, Amyx KK, Ahmann P, Steel EA. Deamidation in human lens βB2-crystallin destabilizes the dimer. *Biochemistry*. 2006;45:3146–3153.
68. Takata T, Oxford JT, Brandon TR, Lampi KJ. Deamidation alters the structure and decreases the stability of human lens βA3-crystallin. *Biochemistry*. 2007;46:8861–8871.
69. Chen J, Callis PR, King J. Mechanism of the very efficient quenching of tryptophan fluorescence in human γD-and γS-crystallins: the γ-crystallin fold may have evolved to protect tryptophan residues from ultraviolet photodamage. *Biochemistry*. 2009;48:3708–3716.
70. Chen J, Flaugh SL, Callis PR, King J. Mechanism of the highly efficient quenching of tryptophan fluorescence in human γD-crystallin. *Biochemistry*. 2006;45:11552–11563.
71. Chen J, Toptygin D, Brand L, King J. Mechanism of the efficient tryptophan fluorescence quenching in human γD-crystallin studied by time-resolved fluorescence. *Biochemistry*. 2008;47:10705–10721.
72. Hanson SR, Hasan A, Smith DL, Smith JB. The major in vivo modifications of the human water-insoluble lens crystallins are disulfide bonds, deamidation, methionine oxidation and backbone cleavage. *Exp Eye Res*. 2000;71:195–207.
73. Hains PG, Truscott RJ. Post-translational modifications in the nuclear region of young, aged, and cataract human lenses. *J Proteome Res*. 2007;6:3935–3943.
74. Hains PG, Truscott RJ. Age-dependent deamidation of lifelong proteins in the human lens. *Invest Ophthalmol Vis Sci*. 2010; 51:3107–3114.

Investigative Ophthalmology & Visual Science